J Solid State Electrochem (2011) 15:293–301
DOI 10.1007/s10008-010-1082-0

ORIGINAL PAPER

Electrically driven oxygen separation through gadolinia-doped ceria using $PrBaCo_2O_{5+x}$ and $NdBaCo_2O_{5+x}$ electrodes

Manoj Yadav · Wenquan Gong · Allan J. Jacobson

Received: 28 March 2010 / Revised: 17 April 2010 / Accepted: 21 April 2010 / Published online: 12 May 2010

Abstract Oxygen gas can be electrochemically separated from ambient air with very high purity and compressed by using a solid-electrolyte ion-transport membrane. An electrolyte with high ionic conductivity such as gadolinium-doped ceria (CGO) and mixed conducting electrodes are used to construct the electrochemical cell. To achieve high oxygen flux, the electrodes must exhibit very fast electrode kinetics. Here, we report the performances of mixed conducting $PrBaCo_2O_{5+x}$ and $NdBaCo_2O_{5+x}$ electrodes in oxygen separation in a planar CGO electrolyte-supported cell. The properties of the electrode materials were evaluated using potentiostatic and potentiodynamic measurements and alternating current impedance spectroscopy. The oxygen flux was also measured using gas chromatography to confirm the absence of gas leaks. The electrodes demonstrated very low polarization resistances as a result of very high cathodic and anodic reaction rates at temperatures of 600–800 °C. High oxygen gas flow rates were observed on applying potentials up to 1 V with an almost linear relationship between the applied potential and the molar flow rate of oxygen gas.

Keywords $PrBaCo_2O_{5+x}$ · $NdBaCo_2O_{5+x}$ · Gadolinia-doped ceria · Oxygen separation membrane · Electrically driven oxygen separation from air

Dedicated to Robert Schöllhorn on his 75th birthday.

M. Yadav
Department of Chemical and Biomolecular Engineering,
University of Houston,
Houston, TX 77204-4004, USA

W. Gong · A. J. Jacobson (✉)
Department of Chemistry, University of Houston,
Houston, TX 77204-503, USA
e-mail: ajjacob@uh.edu

Introduction

Recent advances in the development of mixed electronic–ionic conductors have led to increased interest in electrochemical separation of oxygen gas from air. The electrochemical membrane separation process provides the unique advantage of very high selectivity and purity when compared with conventional separation methods as only O^{2-} ions can transport through the membrane [1]. This important advantage makes electrochemical separation an attractive technology for applications varying from large catalytic reactors for controlled oxidation of hydrocarbons in various chemical processes [2] to small portable medical devices [3]. Oxygen separation can be either pressure-driven or electrically driven.

The pressure-driven design is simpler to fabricate and operate, as a single membrane material with both electronic and ionic conductivity is used without external electrodes. The difference in the partial pressures of oxygen gas on the two sides of the membrane provides the driving force for the separation. A large pressure is applied on the air side (~10 atm) and the permeate side is maintained at lower pressure (<1 atm) to generate enough driving force to obtain high enough flow rates for an economically viable process. In order to produce high-pressure oxygen by this method, an additional compressor is required. In electrically driven membrane separation, the driving force is an externally applied voltage. Thus, air at atmospheric pressure can be used to generate pure oxygen at higher pressures without requiring compressors. The electrically driven separation membrane also has the advantage that the flux can be controlled precisely by varying the applied voltage.

Traditionally, oxygen separators have been fabricated with yttria-stabilized zirconia (YSZ) as the electrolyte,

but YSZ requires high operating temperature (~1,000°C) to achieve adequate ionic conductivity (σ_i~0.1 S/cm). As an example, Ciacchi et al. have successfully constructed a tubular system for oxygen separation based on a YSZ electrolyte [4]. For operation at intermediate temperatures and in the nonreducing environment of oxygen separation, doped ceria electrolytes are good choices for the electrolyte because, unlike YSZ, they do not react with high-performance electrodes containing cobalt such as (La,Sr)CoO_{3-x}. The design of a separation system based on samaria-doped ceria (CSO) electrolyte layers that produced high-pressure oxygen in a single electrochemical step without requiring pumps or compressors was recently reported [5]. Thin CSO electrolyte layers were supported by porous electrodes and by dense layers with microchannels to allow gas contacting with the electrodes. Composite electrodes, comprised of CSO and $La_{1-x}Sr_xCo_{0.2}Fe_{0.8}O_{3-x}$ particles, were used for the cathodic and anodic reactions. The dense layers with microchannels were made from electronically conducting $La_{1-y}Ca_yMnO_3$. High-purity (>99.9%), compressed (2 MPa) oxygen was produced at 750°C in a co-sintered, planar device. In a related study, Meixner et al. have demonstrated long-term stability and reliability of a stack design built with lanthanum strontium cobaltite electrodes and a gadolinia-doped ceria (CGO) electrolyte [6].

The motivation of this research is to design electrodes with enhanced kinetics for oxygen reduction and recombination (low area-specific resistances [ASRs]) to be used in electrically driven oxygen separation at intermediate temperatures (500 to 800°C). The development of cathode materials for low- and intermediate-temperature solid oxide fuel cells has led to the discovery of several materials with fast oxygen reduction kinetics. One family of mixed ionic–electronic conductors $ABaCo_2O_{5+x}$ (ABCO where A = La, Y, Pr, Nd, Sm, Gd, Eu, Y), with the oxygen-deficient A site-ordered double perovskite structure, shows fast oxygen kinetics for intermediate temperatures [7–16]. The ordered perovskites show significantly faster kinetics than the corresponding disordered perovskites. Zhang et al. constructed a separation membrane using different ABCO compounds and determined that $PrBaCo_2O_{5+x}$ (PBCO) has the highest molar flux in pressure-driven membrane separation [17]. They have also shown that PBCO remains stable under low oxygen partial pressure, a condition that might occur during electrode polarization. In this work, the suitability of two examples of the double perovskites, PBCO and $NdBaCo_2O_{5+x}$ (NBCO), has been investigated as electrode materials for electrically driven oxygen separation.

General background

In an oxygen separation membrane, the oxygen reduction reaction $O_2 + 4e^- \rightarrow 2O^{2-}$ takes place at the cathode and the reverse reaction occurs at the anode. The flux of oxide ions or the flux of oxygen molecules can be calculated from the current in the external circuit since $jO_2 = i/(4FA)$ where jO_2 (in moles per square centimeters per second) is the oxygen flux, i (in amperes) is the current, A (in square centimeters) is the electrode area, and F is Faraday's constant. Under open circuit voltage conditions, the cell acts as oxygen concentration cell. The potential across the cell can be calculated using the Nernst equation $E = (RT/4F)\ln(pO_2'/pO_2'')$ with partial pressures of oxygen pO_2' and pO_2'' on either side of the cell provided that the oxygen ion transference number of the solid-electrolyte membrane is equal to unity. This chemical potential gradient results in the transport of oxygen from higher partial pressure (pure oxygen side) to lower partial pressure (air side). To counter this potential, an external potential is applied to provide the driving force for separation of oxygen from air. This applied potential drives the flow of oxygen from the air side to the pure oxygen side, the amount being determined by the current flow. The applied potential is used to work against the Nernst potential, the ohmic resistance of the cell (R), and the overpotentials at the electrodes (η_{cathode} and η_{anode}) arising from the chemical reactions.

The relationship between current density and activation polarization for a single step reaction is given by the well-known Butler–Volmer equation:

$$i = i_0[\exp(\alpha_a nF\eta/RT) - \exp(-\alpha_c nF\eta/RT)]$$

where i_0 is the exchange current density, α is a charge transfer coefficient (α_a and α_c), η is the overpotential, n is the number of electrons, and the other symbols have their usual meanings.

This equation can be approximated for higher polarizations by the Tafel equation where the anodic or cathodic overpotentials are given by $\eta = (RT/\alpha nF)\ln(i) - (RT/\alpha nF)\ln(i_0)$. For very low polarizations, the equation can be further approximated to $\eta = (RT/\alpha nF)(i/i_0)$. At very high current densities, mass transfer rate limitations of reactant and product oxygen molecules associated with diffusion through the porous electrodes occur. The concentration polarization can be expressed as $\eta_{\text{conc}} = (RT/nF)(i_l - i/i_l)$ where i_l is the limiting current density. The value of limiting current density depends on partial pressure of oxygen and electrode microstructure and can be determined experimentally.

Thus, the applied potential can be written as the sum of all polarization losses as follows: $V_{appl} = E + iR + \eta_{activation} + \eta_{concentration}$.

Experimental

Sample preparation

The CGO powder (purchased from Anan Kasei Co. Ltd., Japan) was die-pressed into a pellet and sintered at 1,450 °C for 8 h in air. The diameters of the sintered pellets were 19 mm. The thickness of the CGO electrolyte pellets was reduced to 0.5–0.7 mm by polishing with SiC paper. A composite of ABCO-CGO (50 wt.%) (where A = Pr, Nd) was used to make the electrodes. The ABCO powders were prepared by mixing stoichiometric amounts of $BaCO_3$, Co_3O_4, and Pr_6O_{11} or Nd_2O_3 in a ball mill and heating in a platinum crucible at 1,050 °C for 5 h in air. The powders thus obtained were confirmed to be single phase by powder X-ray diffraction. The ABCO-CGO pastes were prepared from powder mixtures of ABCO and CGO in terpineol. A thin ABCO-CGO layer with a diameter of 12.7 mm was first applied to both sides of the CGO electrolyte pellet and then fired at 1,070 °C for 2 h in air. A second layer of ABCO-CGO paste was subsequently applied to the surface of the sintered ABCO-CGO layer and fired at 1,050 °C for 2 h in air to increase the thickness of the electrode. A two-layer structure reduces the effect of thermal expansion coefficient mismatch and also gives a thin dense layer of electrode near the electrolyte surface and a porous electrode layer on the outside.

The geometric areas of the cathode and anode were each 1.27 cm^2. Since Pt catalyzes the oxygen reduction reaction, two pieces of gold mesh were used as current collectors and bonded onto both surfaces of the electrodes by firing with gold paste at 700 °C for 0.5 h in air.

The microstructure of the electrodes is shown in Fig. 1. The electrodes were ~35 μm thick. The thickness of the outer porous layer was ~20 μm and that of the relatively dense inner layer was ~15 μm.

Experimental arrangement

The membranes were sealed against an alumina tube using gold O-rings on a spring-loaded sample holder. The configuration of the experimental setup is shown in Fig. 2. A four-wire configuration was used to minimize the effect of wire resistance. Two wires are current carrying and the other two noncurrent-carrying wires are used to measure or apply voltage at the electrodes. The outer side of the sample was exposed to air. The other side was purged with pure helium gas, and the oxygen and helium gas

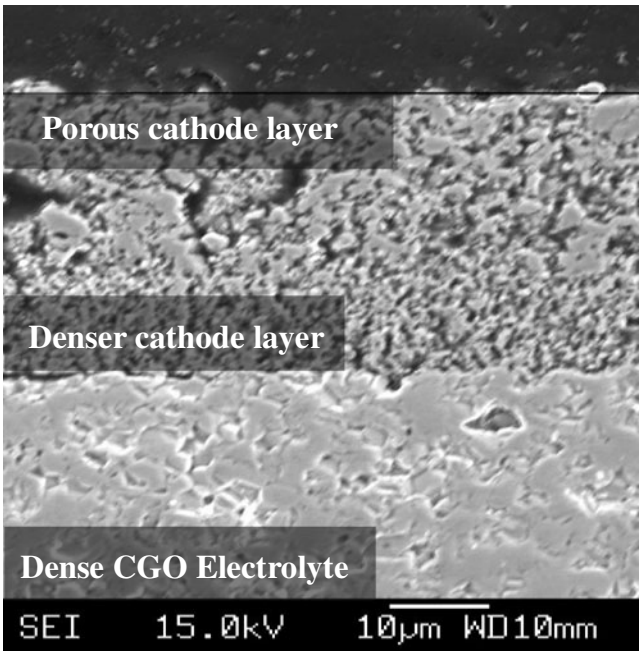

Fig. 1 A secondary electron image of the PBCO-CGO electrode structure showing the two PBCO-CGO layers

mixture exiting the apparatus was brought to the gas chromatograph for analysis. Helium was used as sweep gas for gas chromatography with a flow rate of 100 cm^3 min^{-1}. A thermocouple was placed very close to the sample on the helium side. An Antek 3000 gas chromatograph was used for gas analysis and a Solartron 1260 impedance analyzer in conjunction with Solartron 1287 electrochemical interface were used for voltage application, current measurements, and impedance spectroscopy. Impedance spectroscopy was used to separate the ohmic and polarization resistances. The electrodes were made to have the same size and alignment to avoid errors associated with misalignment and area difference.

Oxygen separation

The oxygen separation experiments were conducted by applying different voltages across the cell and measuring both the current and separately the oxygen gas concentration in the helium sweep gas while keeping the voltage constant. The oxygen gas concentration was measured only after a steady-state current was achieved. The gas chromatography method was utilized to make sure that no leaks were present in the system and that all of the oxygen present in the He stream was accounted for by the current measurements.

In an air separation experiment, oxygen from air is pumped through the membrane to give a stream of pure oxygen gas at a pressure of 1 atm or higher. To assess the performance of the cell under these conditions, the oxygen

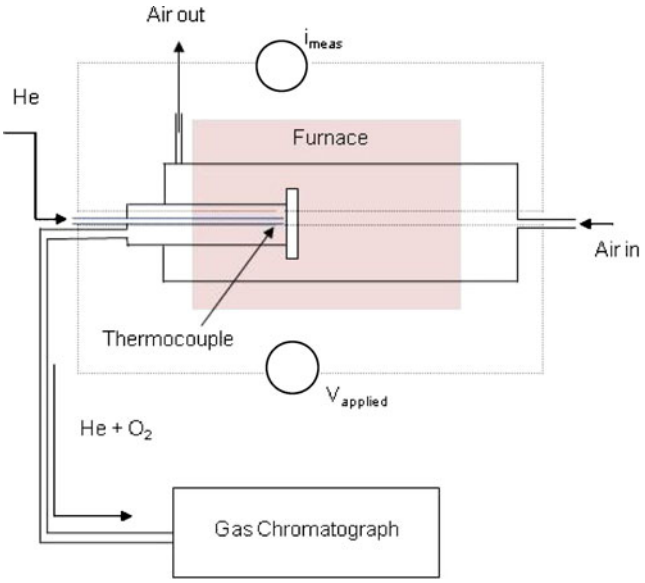

Fig. 2 A schematic diagram of the oxygen separation experimental arrangement

flux was measured at different applied voltages with air on one side and pure oxygen on the other. The oxygen flux was determined from measurements of the current at different voltages. The ohmic and polarization resistances of the electrochemical cell were determined by alternating current (AC) impedance spectroscopy.

Results

Oxygen separation

Measurement of the amount of nitrogen present on the permeate side indicated that the air leak was small (<0.05% at low helium flow rates, even lesser at higher helium flow rates). The small leakage was taken into account in the oxygen flux calculations. The flux was also calculated independently from the measured current using the relationship $j(O_2) = i/(4FA)$ where A is the active membrane area. The oxygen flux calculated by both methods for a PBCO-CGO cell in the temperature range of 500 to 700 °C is shown in Fig. 3. Excellent agreement was obtained between the measured oxygen fluxes and the flux values calculated from current.

In this experiment, the electrode polarization resistance of the electrode on the helium side is expected to be high due to the very low oxygen partial pressure and, consequently, the fluxes are not the highest that can be achieved. The agreement between oxygen fluxes determined from the current measurements and by gas chromatographic analysis confirms the validity of the experimental approach.

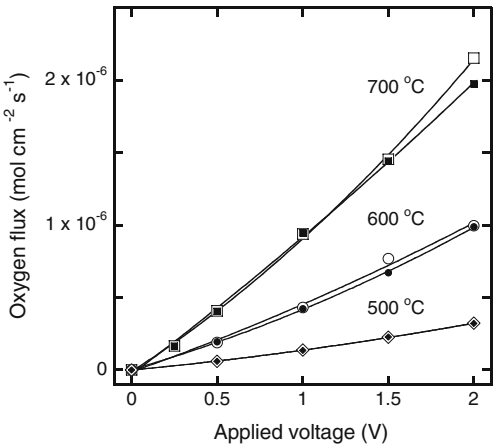

Fig. 3 Variation of the oxygen flux with the applied voltage at three temperatures. The *open* and *closed symbols* correspond to the values determined by current and gas chromatography measurements, respectively

Air separation

The results for the oxygen flux measurements using PBCO and NBCO electrodes are shown in Fig. 4. The electrolyte thickness was 0.6 mm for the NBCO experiment and 0.55 mm for the PBCO experiment. The molar flux varies almost linearly with applied voltage because the largest contribution towards total resistance is the ohmic part. The maximum oxygen molar flux observed was 2.48×10^{-6} mol cm^{-2} s^{-1} at 800 °C and at an applied voltage of 1 V for the PBCO-CGO composite electrode with a 0.55-mm-thick electrolyte. Measurements were made only after a stable current value was achieved at a certain applied potential. The current values are stable for the applied voltage range of 0 to 1 V but an applied potential higher than 1 V leads to

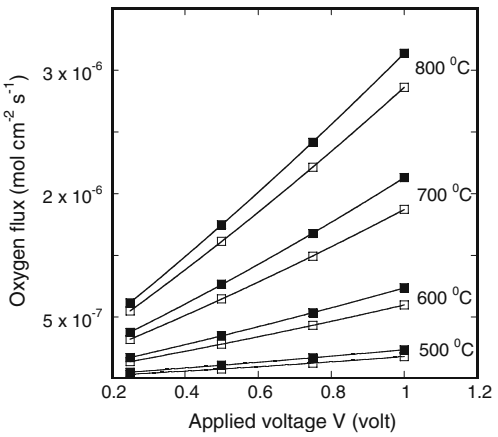

Fig. 4 Variation of the oxygen flux with the applied voltage at different temperatures. The *closed symbols* correspond to the values determined by current measurements for PBCO-CGO electrodes and a 0.55-mm-thick electrolyte; the *open symbols* correspond to NBCO-CGO electrodes with a 0.6-mm-thick electrolyte

increased polarization resistance over time which might be caused by electrode decomposition.

At low applied potential and lower temperature, the variation of the oxygen flux with applied potential is nearly linear, indicating that the ohmic resistance from the electrolyte is the largest contribution under these conditions. Some deviation is apparent at higher applied potential due to internal resistive heating. The flow rate corresponding to 1 V at 800°C is higher than expected because the large current density (~1 A/cm^2) generates heat (i^2R) which slightly raises the temperature of the sample above the furnace set point. The localized heating of the sample reduces the electrolyte resistance and leads to even higher current density. The heating effect is more pronounced at higher temperatures and for thinner electrolytes because the Joule heating is proportional to the square of the current and current increases with increasing temperature and decreasing electrolyte thickness. This heating could be useful in designing future devices that can start at lower temperature and can reduce the external heating requirement.

AC impedance measurements

To assess the performance of the individual components of the cell, impedance spectroscopy measurements were made on the cell in a frequency range of 0.001 to 100,000 Hz using a small AC perturbation of 25 mV. Impedance spectra in the form of Nyquist plots for the cell configuration with CGO electrolyte and PBCO-CGO electrodes with pure oxygen at 1 atm on one side and air on the other side at different temperatures are shown in Fig. 5. The high-frequency intercept represents the ohmic resistance, which includes resistances associated with electrolyte and wires. The low-frequency intercept includes the electrode polarization resistance and the ohmic resistance of the electrolyte and wires. To obtain the ASRs of the electrode, the difference between the low-frequency and high-frequency intercepts was taken and multiplied by the electrode area.

The impedance spectra were analyzed to separate the resistance contributions from different parts of the cell. The variations of ohmic, polarization, and total ASRs with temperature for the cell with PBCO-CGO electrodes are shown in Fig. 6. The ASRs were extracted from the impedance spectroscopy as described above and averaged to get resistance values for the half cell. It is apparent that, in the temperature range 500 to 800°C, the ohmic resistance is the major contributor towards the total resistance, and even higher flux rates can be achieved by reducing the thickness of electrolyte.

Both PBCO-CGO and NBCO-CGO electrodes show very small ASRs. Direct comparison of ASRs for different materials is difficult because, apart from the catalytic properties of the electrode material, the ASR depends upon various other factors such as particle size, porosity, electrode thickness, electrode composition, electrolyte material, and electrode preparation method. However, the data show that non-optimized ASRs of the ABCO-CGO electrodes (0.21 Ohm cm^2 at 600°C for PBCO-CGO electrodes) are lower in comparison to the results obtained for LSF-CSO where, at 750°C, the ASR of small coupons without the gas manifold layers was typically 0.25 Ohm cm^2 [5]. A 150°C lower temperature is indicative of faster oxygen reduction reaction kinetics.

Kinetic parameters

The kinetic parameters can be extracted from the impedance spectra for a mixed conducting electrode where solid-state oxygen diffusion and oxygen surface exchange kinetics dominate the electrochemical behavior, using the Adler, Lane, and Steele (ALS) model [18, 19]. The ALS model was developed for a symmetric cell with two identical electrodes with the same gas atmosphere on both sides. In our case, the electrodes were identical but the gas atmospheres were different, so we extended the model to the sum of two half cell electrodes with different kinetic parameters. The other assumptions and definitions remain the same as in the ALS model.

For the oxygen separation experiment, the total impedance can be expressed as the sum of two half cell chemical impedances: $Z = R_{\text{electrolyte}} + Z_{\text{interface}} + Z_{\text{chem1}} + Z_{\text{chem2}}$ where Z_{chem}, the impedance of individual electrode reaction, is:

$$Z_{\text{chem}} = R_{\text{chem}} \sqrt{\frac{1}{1 + j\omega t_{\text{chem}}}} \tanh\left(\frac{\lambda}{\delta} \times \sqrt{1 + j\omega t_{\text{chem}}}\right)$$

where R_{chem} is a characteristic resistance, t_{chem} is a characteristic time constant, L is the thickness of the electrode, and δ is a characteristic length that determines the transition from bulk to surface control of the reaction kinetics.

The Nyquist plots from the experiment are in the form of a single depressed semicircle. No features from interfacial or grain boundary resistances at medium frequencies are observed; PBCO and NBCO compounds do not react with CGO to form nonconducting interfaces. Thus, the equivalent circuit shown in Fig. 7 can be used to represent the system and fit the impedance data. Here, L is the inductance associated with measurement lead wires (which has negligible effect at lower temperatures), R is associated with the electrolyte, and Z_{chem1} and Z_{chem2} are electrode impedances associated with the two electrodes:

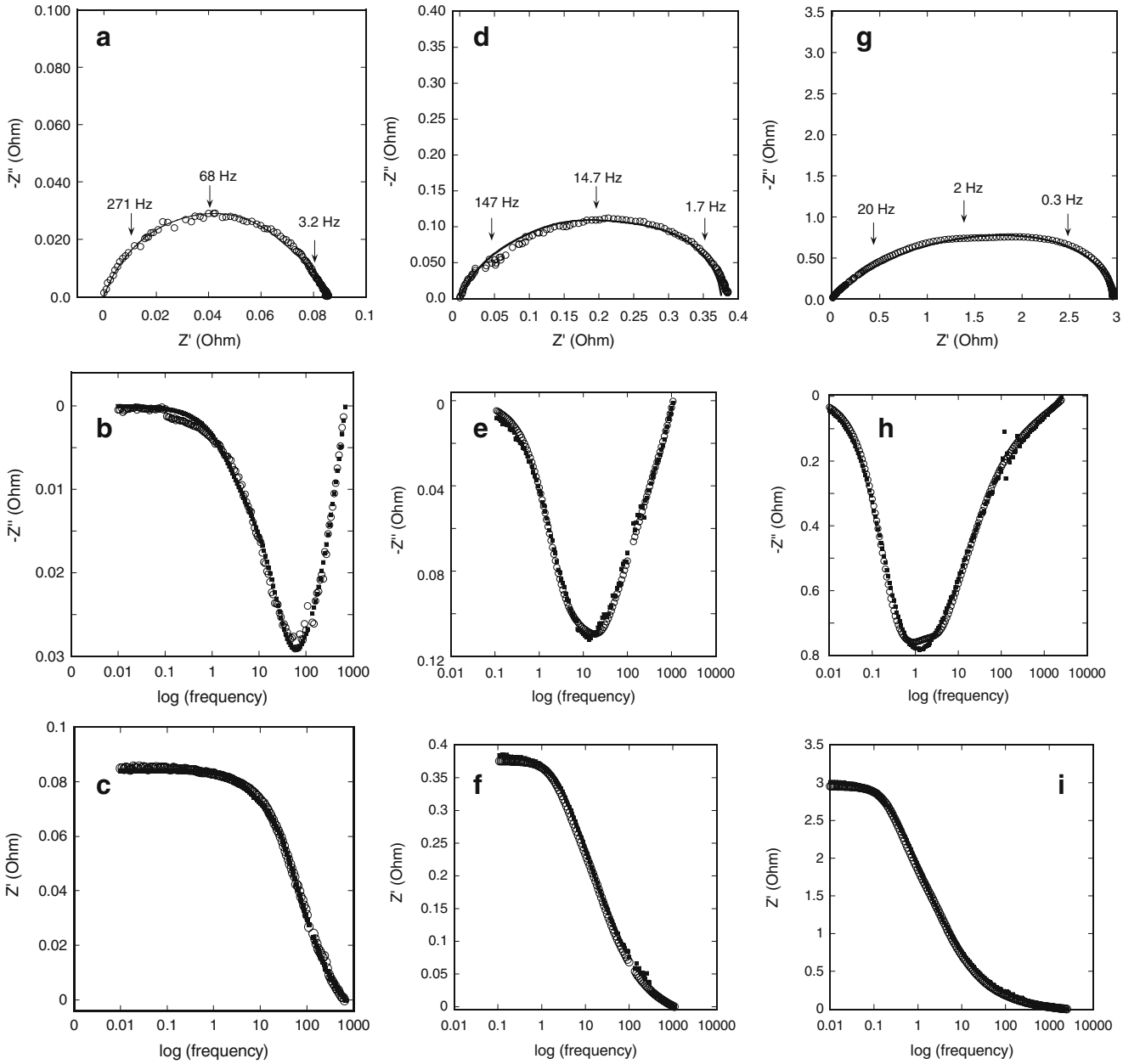

Fig. 5 Impedance spectra of symmetric PBCO-CGO cell with oxygen and air on either sides: **a**, **b**, **c** 500 °C; **d**, **e**, **f** 600 °C; **g**, **h**, **i** 700 °C. In **a**, **d**, **g**, the *open circles* represent experimental data and the *solid line* represents fitting data. In **b**, **c**, **e**, **f**, **h**, **i**, the *open symbols* are the measurements and the *filled symbols* are the fitted points

one on the oxygen side and the other on the air side. Each Z_{chem} was defined in terms of R_{chem}, t_{chem}, and δ. Altogether, eight parameters were used to fit the impedance spectra using nonlinear least squares. Several sets of initial values were used to avoid the possibility of local minima. The results of fitting both PBCO-CGO and NBCO-CGO electrode responses are given in Table 1. The model fits the data well as shown by the agreement between the observed and calculated results for the PBCO-CGO electrode (Fig. 5). Furthermore, the values determined for the electrolyte resistance are in good agreement with the values calculated from the electrolyte dimensions and the literature data.

In principle, the parameters extracted from the data (R_{chem} and t_{chem}) listed in Table 1 can be further analyzed to determine the bulk diffusion and surface exchange coefficients (D_{chem} and k_{chem}) in the context of the ALS model. This analysis is not made here because it requires further

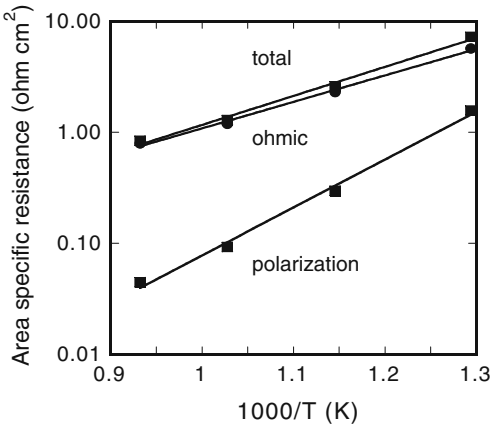

Fig. 6 Ohmic and polarization resistance contributions towards total ASR for the cell with PBCO-CGO electrodes

assumptions concerning the contribution of the CGO used in the composite electrodes to the electrode reactions. A detailed knowledge of the three-phase electrode microstructure is also required.

Analysis of the *i–V* data

Potentiodynamic data cannot be determined in the usual way by applying a voltage sweep to the sample because the temperature continually increases with applied voltage due to resistive heating discussed earlier. To avoid the effect of changing temperature, another approach was used. A fixed potential (0.25, 0.5, 0.75, and 1 V) was applied for a short period of time (<5 s) and data were collected at 10 Hz. The current reached a constant value in less than a second and then began to increase as the temperature started to rise. The constant value of the current is taken as the true response in absence of resistive heating. These current values were used in modeling the *i–V* data.

The parameters obtained from the impedance spectroscopy, as described in the last section, were used to predict the potentiodynamic behavior of the system; the following analysis shows the correlation between model predictions and experimental data.

The exchange current density i_0 can be approximated from the results of the impedance analysis. For the very small voltage perturbation used in the impedance measurements, the Butler–Volmer equation can be approximated as $\eta=(RT/\alpha nF)(i/i_0)$. This equation can be rearranged in terms of the area-specific resistance R_{ASR} to give i_0 as follows [20]:

$$i_0 = \frac{RT}{R_{\mathrm{ASR}} 2\alpha F}.$$

The impedance spectra for the air and oxygen sides were plotted as Nyquist plots from the Z_{chem1} and Z_{chem2} data, and the R_{ASR} was calculated from the real axis intercepts as described earlier. We assumed transfer coefficients for both the anodic and cathodic reactions to be equal, thus, $\alpha_{\mathrm{c}} = \alpha_{\mathrm{a}} = 0.5$.

The exchange current densities calculated by this method are shown in Fig. 8 together with results for a LSM-YSZ electrode [20]. The figure shows that the exchange current densities for ABCO-CGO electrodes are significantly larger at intermediate temperatures than observed for LSM-YSZ electrodes. The activation energies were also smaller for both NBCO-CGO (~123 kJ/mol) and PBCO-CGO (~107 kJ/mol) electrodes compared to the LSM-YSZ composite (~151 kJ/mol).

The exchange current densities for individual electrodes can thus be used to calculate polarization losses at each electrode. The electrode polarization loss for α=0.5 and n=2 can be obtained from rearranging the Butler–Volmer equation to give:

$$\eta_{\mathrm{polarization}} = \frac{RT}{F}\sinh^{-1}(i/2i_0) = \frac{RT}{F}\ln\left[\frac{i+\sqrt{i^2+4i_0^2}}{2i_0}\right].$$

For large exchange current densities, the electrode polarization losses will be smaller and, thus, we expect very small polarization losses for these electrodes. This equation was used to model the system; concentration polarization losses were observed to be negligible. The overpotential can be written as: $\eta_{\mathrm{polarization}} = V_{\mathrm{appl}} - E - \eta_{\mathrm{ohmic}}$ where V_{appl} and E are measured quantities and $\eta_{\mathrm{ohmic}}=iR_{\mathrm{ohmic}}$ and R_{ohmic} and i_0 were obtained from the impedance data. The quantity $\left(V_{\mathrm{appl}} - E - \eta_{\mathrm{ohmic}}\right)$ can be considered as an experimental measurement of polarization losses while $\eta_{\mathrm{polarization}}$ can be calculated as sum of polarization losses at both electrodes. A comparison of calculated and measured electrode polarization losses at the electrodes is shown in Fig. 9 and the model shows really good agreement with experimental data for both NBCO-CGO and PBCO-CGO electrodes in the entire temperature range. The figure also shows that electrode polarization losses increase with decreasing temperature, but these losses are very small compared to ohmic losses.

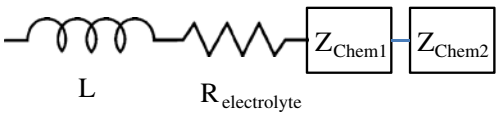

Fig. 7 Equivalent circuit for the electrochemical separation system

Table 1 Fitting parameters for the impedance data for PBCO-CGO and NBCO-CGO electrodes on a CGO electrolyte; electrodes 1 and 2 correspond to the electrodes at pO_2=1 and 0.1 atm, respectively

	T (°C)	$R_{electrolyte}$ (Ohm)	L (cm)	t_{chem} (s)	L/δ	R_{chem} (Ohm)
PBCO-CGO				Electrode 1		
	500	9.166	2.08E−06	0.0374	1.729	0.769
	600	3.366	3.9E−06	0.0057	1.735	0.114
	700	1.637	4.98E−06	0.0018	2.229	0.052
				Electrode 2		
	500			0.492	2.282	1.879
	600			0.051	2.450	0.228
	700			0.017	2.437	0.033
NBCO-CGO				Electrode 1		
	500	9.843	3.61E−07	0.1789	1.724	2.076
	600	3.645	2.15E−06	0.0213	1.774	0.347
	700	1.828	3.31E−06	0.0036	1.707	0.084
				Electrode 2		
	500			1.8318	2.384	4.9392
	600			0.1501	2.621	0.5266
	700			0.0298	2.441	0.0772

For example, for the PBCO-CGO cell at 700 °C and a current density of 0.587 A/cm^2, the ohmic loss was 0.95 V whereas electrode polarization loss was 0.05 V. From this analysis, we can deduce that, for such an electrochemical oxygen separation cell, with these novel electrode materials, the cell performance is limited by the thickness of the electrolyte. This is shown by the fact that the combined effect of reducing the thickness of the electrolyte by almost 8.5% and changing the electrode material from NBCO-CGO to PBCO-CGO produced an almost 10% improvement in performance. Use of a thinner electrolyte membrane will further enhance the oxygen flux.

Conclusions

PBCO and NBCO were successfully employed as novel electrode materials for electrochemical oxygen separation from air. These materials exhibit very low polarization resistances and CGO electrolyte-based cells show very high fluxes of oxygen gas in the temperature range 600 to 800 °C. The oxygen fluxes were analyzed using gas chromatography and potentiodynamic methods and the electrode performance was analyzed using impedance spectroscopy. The ASL model was used to model the impedance spectroscopy response. The electrode kinetics are very fast for both PBCO-CGO and NBCO-CGO

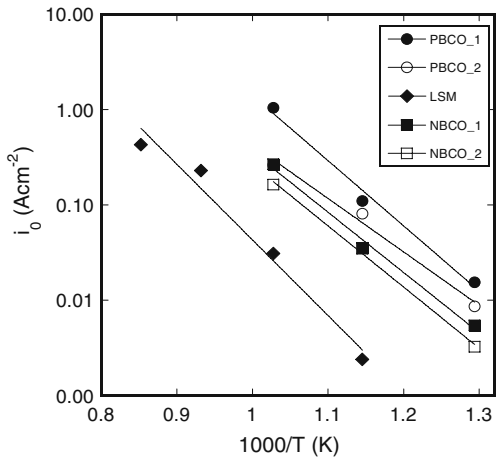

Fig. 8 Exchange current density comparison of PBCO-CGO, NDCO-CGO, and LSM-CGO composite electrodes. The LSM-YSZ data are from reference [20]; *1* and *2* refer to the oxygen and air sides of the cell

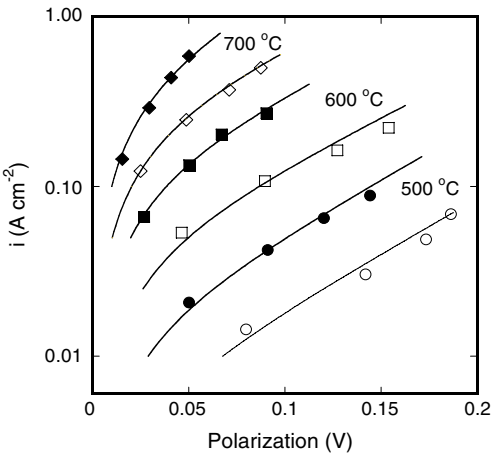

Fig. 9 Variation of polarization losses at electrodes with current density. The *open* and *closed symbols* represent NBCO-CGO and PBCO-CGO electrodes, respectively. The *solid line* represents model fitting

electrodes and the oxygen molar flux is determined largely by the electrolyte thickness. Reducing the thickness of the electrolyte by a factor of 10 to ~50 μm will increase the oxygen flux by a factor of 4 to 7 depending on the operating temperature.

Acknowledgements This research was supported by the Robert A. Welch Foundation, Seprox Inc. (synthesis and characterization of materials), US Department of Energy, Office of Basic Energy Sciences, Division of Materials Sciences and Engineering under Award No. DE-SC0001284 (electrochemical measurements).

References

1. Bouwmeester HJM, Burggraaf AJ (1997) Dense ceramic membranes for oxygen separation. In: Gellings PJ, Bouwmeester HJM (eds) The CRC handbook of solid state electrochemistry. Boca Raton, CRC, pp 481–553
2. Pfaff EM, Zwick M (2008) Ceram Eng Sci Proc 28:23–31
3. Badwal SPS, Ciacchi FT (2001) Adv Mater 13:993–996
4. Ciacchi FT, Badwal SPS, Zelizko V (2002) Solid State Ion 152–153:763
5. Hutchings KN, Bai J, Cutler RA, Wilson MA, Taylor DM (2008) Solid State Ion 179:442–450
6. Meixner DL, Brengel DD, Henderson BT, Abrardo JM, Wilson MA, Taylor DM, Cutler RA (2002) J Electrochem Soc 149: D132–D136
7. Taskin AA, Lavrov AN, Ando Y (2005) Appl Phys Lett 86:091910/1–091910/3
8. Kim G, Wang S, Jacobson AJ, Yuan Z, Donner W, Chen CL, Reimus L, Brodersen P, Mims CA (2006) Appl Phys Lett 88:024103/1–024103/3
9. Chang A, Skinner SJ, Kilner JA (2006) Solid State Ion 177:2009–2011
10. Kim G, Wang S, Jacobson AJ, Reimus L, Brodersen P, Mims CA (2007) J Mater Chem 17:2500–2505
11. Tarancon A, Skinner SJ, Chater RJ, Hernandez-Ramirez F, Kilner JA (2007) J Mater Chem 17:3175–3181
12. Gong W, Yadav M, Jacobson AJ (2009) Mater Res Soc Symp Proc 1126:130
13. Kim J-H, Manthiram A (2008) J Electrochem Soc 155:B385–B390
14. Kim J-H, Prado F, Manthiram A (2008) J Electrochem Soc 155: B1023–B1028
15. Zhou Q, He T, He Q, Ji Y (2009) Electrochem Commun 11:80–83
16. Kim JH, Cassidy M, Irvine JTS, Bae J (2009) J Electrochem Soc 156:B682–B689
17. Zhang K, Ge L, Ran R, Shao Z, Liu S (2008) Acta Mater 56:4876–4889
18. Adler SB, Lane JA, Steele BCH (1996) J Electrochem Soc 143:3554–3564
19. Adler SB (1998) Solid State Ion 111:125–134
20. Co AC, Xia SJ, Birss VI (2005) J Electrochem Soc 152:A570–A576